Published in final edited form as:
J Mol Biol. 2007 October 26; 373(3): 755–763. doi:10.1016/j.jmb.2007.08.043.

STRUCTURAL AND KINETIC CHARACTERIZATION OF QUINOLINATE PHOSPHORIBOSYLTRANSFERASE (hQPRTase) FROM *HOMO SAPIENS*

Huanting Liu, **Kerry Woznica**, **Gemma Catton**, **Amanda Crawford**, **Nigel Botting**, and **James H. Naismith**[*]
The Centre for Biomolecular Science, The University of St Andrews, North Haugh, St. Andrews KY16 9ST

Abstract

Human quinolinate phosphoribosyltransferase (EC 2.4.2.19) (hQPRTase) is a member of the type II phosphoribosyltransferase family involved in the catabolism of quinolinic acid. It catalyses the formation of nicotinic acid mononucleotide from quinolinic acid, which involves a phosphoribosyl transfer reaction followed by decarboxylation. hQPRTase has been implicated in a number of neurological conditions and in order to study it further, we have carried out structural and kinetic studies on recombinant hQPRTase. The structure of the fully active enzyme overexpressed in *E. coli* was solved using multiwavelength methods to a resolution of 2.0 Å. hQPRTase has a α/β barrel fold sharing a similar overall structure with the bacterial QPRTases. The active site of hQPRTase is located at an α/β open sandwich structure that serves as a cup for the α/β barrel of the adjacent subunit with a QA binding site consisting of three arginine residues (R102, R138 and R161) and two lysine residues (K139 and R171). Mutation of these residues affected substrate binding or abolished the enzymatic activity. The kinetics of the human enzyme are different to the bacterial enzymes studied, hQPRTase is inhibited competitively and non-competitively by one of its substrates, PRPP. The human enzyme adopts a hexameric arrangement which places the active sites in close proximity to each other.

Keywords

NAD biosynthesis; *Homo sapiens* quinolinate phosphoribosyltransferase (hQPRTase); quinolinic acid (QA); 5-phosphoribosylpyrophosphate (PRPP); nicotinic acid mononucleotide (NAMN); mutagenesis; kinetics

Introduction

Quinolinic acid (QA) plays a key role in the *de novo* biosynthesis of nicotinamide adenine dinucleotide (NAD) which proceeds from tryptophan, aspartic acid and glycerol or related compounds depending on the specific system [1]. In mammals, QA is a potent endogenous excitotoxin to neuronal cells, causing neuronal damage through sustained activation of glutamate N-methyl-D-aspartate receptors. Elevation of QA levels in the brain has been linked to the pathogenesis of a range of neurodegenerative disorders [2; 3; 4].

[*]Corresponding Author Address: The Centre for Biomolecular Science, BMS Building The University of St Andrews, North Haugh, St. Andrews KY16 9ST Fife, Scotland, UK Tel: (44) 1334 46 Fax: (44) 1334 462595 naismith@st-andrews.ac.uk Tel: (44) 1334 463792 Fax: (44) 1334 462595 .

Europe PMC Funders Author Manuscripts

QA is synthesized by 3-hydroxyanthranilic acid oxygenase (EC 1.12.11.6) which catalyzes the oxidative cleavage reaction of 3-hydroxyanthranilic acid (3-HA) to α-amino-β-carboxymuconate-ε-seminaldehyde (ACMS), which then spontaneously cyclizes to form QA (Figure 1). The activity of 3-hydroxyanthranilic acid oxygenase is known to increase in Huntington's disease patients [3; 4] and in mice as a result of epilepsy 5; 6. QA levels are reduced by quinolinate phosphoribosyltransferase (QPRTase) (EC 2.4.2.19) which catalyses the transfer of the phosphoribosyl moiety from phosphoribosyl pyrophosphate (PRPP) to QA yielding nicotinic acid mononucleotide (NAMN), pyrophosphate and CO_2, to provide the *de novo* source of NAMN for NAD biosynthesis (Figure 1).

QPRTase belongs to the phosphoribosyltransferase (PRTase) group of enzymes that catalyze the formation of *N*-nucleoside bonds in purine, pyrimidine, and pyridine nucleosides. Nucleotide formation involves inversion of stereochemistry at the anomeric ribose C_1, which is proposed to proceed *via* a transition state with considerable oxocarbonium character at the $C_1$1-O_4 of ribose [7]. Based on the active site architecture, PRTases are classified into two distinct evolutionary groups. The first group, the type I PRTase enzymes which includes OPRTase [8], HGPRTase [9], glutamine PRPP amidotransferase (GPAT) [10], UPRTase [11] and PRPPase[12] have an active site architecture involving a Rossman fold and a solvent-exposed active site[13; 14]. The second group of PRTase, the type II enzymes, is represented by QPRTase. Structure determination of QPRTases from *Salmonella typhimurium* (St-QPRTase) [13], *Mycobacterium tuberculosis* (Mt-QPRTase) [15], *Helicobacter pylori* (Hp-QPRTase) [16], *Thermus thermophilus* (Tt-QPRTase) (PDB code 1x1o) and *Thermotoga maritime* [17] (Tm-QPRTase) show that QPRTase an unusual seven-stranded α/β barrel. The active site is located within the barrel and requires the other subunit of an intimate dimer to complete its formation. QA is bound at the base of a solvent-occluded active site while PRPP is positioned between QA and the solvent.

QPRTase is ubiquitous and has been isolated from bacteria [18; 19], plants [1; 20; 21; 22] and mammalian liver and brain [5; 23; 24; 25; 26]. The decarboxylation which occurs along with the phosphoribosyl transfer [27] is essentially an irreversible step. Kinetic analysis of QPRTase from *E. coli* reported an ordered substrate binding mechanism in which PRPP binding is followed by QA binding [28]. However further analysis of QPRTase from *S. typhimurium* showed that the enzyme follows an ordered substrate binding mechanism in which binding of QA precedes PRPP binding [29]. The second possibility is compatible with the known structure of the QPRTase-ligand complex [15]. Structure determination of St-QPRTase in complex with QA and NAMN [13], and Mt-QPRTase [15] gave further insights into the enzymatic mechanism. The human enzyme conserves the key active site residues and has sequence identity ranging from 29% (St-QPRTase) to 41% (Tt-QPRTase) with the bacterial enzymes of known structure. The human enzyme [25], like other mammalian QPRTases [23; 30], is thought to be hexamer. Most enzymatic and structural analysis of mammalian QPRTase has been carried out using the enzyme purified from the host tissue [24; 25; 31; 32] which limited the detailed biochemistry that was possible. Active recombinant hQPRTase has been expressed in *E. coli* cells [33].

We report the structure and kinetic evaluation of recombinant hQPRTase to a resolution of 2.0 Å. This structure locates the active site and combined with site directed mutagenesis identifies the key residues in catalysis. Kinetic analysis suggests hQPRTase may regulate its activity by complex substrate inhibition.

Results

The hQPRTase structure

Crystals of the apo-hQPRTase diffracted to a resolution of 2.0 Å in space group $P2_12_12_1$ and analysis of solvent content suggested the asymmetric unit would contain between 10 and 14 monomers. The expressed protein runs on a gel filtration column with a retention time consistent with a hexamer. A hexamer in solution has also been observed for QPRTases from other mammals such as hog [23], rat [30] and human [25]. We expected the asymmetric unit would contain two hexameric units. However, all attempts to solve the structure by molecular replacement using the bacterial enzymes (monomers, dimers and hexamers) as search models failed. The structure was solved by a combination of multi-wavelength anomalous dispersion phasing and non-crystallographic averaging. The asymmetric unit of the crystal contained 12 monomers of protein, arranged as two hexamers. The final model had no residues in the disallowed regions of the Ramachandran plot.

The monomer of hQPRTase is similar to that of the bacterial enzyme comprising 12 β strands and 11 α helices arranged into two domains (Figure 2A). The N-terminal domain (residues 1-112 and 279-291) is composed of a four-stranded β1, β3, β5 and β12 anti-parallel β sheet stacked against helices α l, α2, α3, α4 and part of the 33 residue long α5. The strands β1 and β3 are followed by 2 short strands β2 and β4 forming a small two-stranded antiparallel β sheet. The C-terminal domain (residues 113-278) is an α/β-barrel structure consisting of the remaining strands β6, β7, β8, β9, β10 and β11 and 8 α helices (α5, α6, α7, α8, α9, α10, α11 and α12) arranged in $(\alpha/\beta)_2\alpha(\alpha/\beta)_5$ topology. The domains are connected by α5 and α12. hQPRTase superimposes most closely with the enzyme from *T. thermophilus* (PDB code 1x1o) with an rmsd of 1.5 Å for 268 matching Cα atoms. Similar results are obtained with other bacterial structures, the most structurally divergent is the enzyme from *S. typhimurium* [13] with an rmsd of 2Å for 259 Cα atoms. Superposition of QPRTase monomers is shown in On-line Supporting Materials (1).

Six (AB) dimers can be identified in the asymmetric unit of the hQPRTase crystal structure. This is the canonical dimer seen in all bacterial enzyme structures. The AB dimer is formed by a two-fold rotation that places the N-terminal domain of one monomer next to the C-terminal domain of the other (Figure 2B) and buries 4900 $Å^2$, 18% of total surface area (similar to the surface area buried by dimers in the structures of bacterial QPRTase). The predicted active site is located at the interfaces between the α/β barrel of one monomer and the β sandwich of the second monomer. Each canonical dimer is related to two other dimers by a three fold rotation axis which gives rise to a hexameric arrangement with D3 symmetry (Figure 2C), essentially identical to Hp-QPRTase and Tt-QPRTase arrangements. In the hexamer, each molecule makes quite extensive contacts with three other monomers. These additional “dimer dimer” interactions bury a further 12000 $Å^2$ of surface per hexamer. Analysis of the hexamer by the program PISA [34] confirms the hexameric assembly is energetically stable. Gel filtration data showed that hQPRTase was hexameric in solution in agreement with the observed hexameric form in the crystal. The contacts between the two hexamers in the asymmetric unit bury only a further 700 $Å^2$ and when scored by the program PISA[34] a dodecamer is unstable. The most extensive crystal contact between monomers from different asymmetric units buries 1028 $Å^2$.

Active site

The QA-binding site of QPRTases is in a deep, solvent accessible, pocket located at the centre of the α/β barrel. In the hQPRTase structure, this surface is composed of R102*, R138, K139, H159, R161 and K171 (* denotes from other subunit in the canonical dimer). These residues are conserved amongst QPRTases and adopt similar conformations in the

bacterial enzymes (Figure 3). These residues create an intensely electrostatically positively charged surface at the centre of the barrel. In the hQPRTase structure, the QA-binding site is occupied by a tartrate molecule which mimics at least in part QA (Figure 2D).

Kinetic analysis

Steady-state kinetic analysis of hQPRTase was carried out using a continuous UV-assay which monitored the appearance of product. The kinetic parameters for QA were initially determined at 0.1mM PRPP and found to be K_m = 21.6 ± 3.0 μM and V_{max} = 1.19 ± 0.05 μM min^{-1}. The specific activity was 0.09 μmol min^{-1} mg^{-1}, which is of the same order of magnitude as data reported for bacterial QPRTases[13; 26; 29]. The kinetic data for QA were re-measured at different PRPP concentrations, showing a small decrease in Km and a large increase in V_{max} with increasing PRPP concentration. The double reciprocal plots for these data were observed to intersect to the right of the vertical axis, which indicated that the affinity of hQPRTase for QA is independent of the PRPP concentration (Figure 4A) indicating that QA binds to the enzyme before PRPP. Kinetic studies with PRPP as the variable substrate, with QA fixed at 0.3 mM, showed pronounced product inhibition above 0.3 mM PRPP. However, taking measurements in the range 0.01 to 0.3 mM PRPP gave a K_m of 23.2 ± 3.6 μM and V_{max} of 0.93 ± 0.03 μM min^{-1}. When the QA concentration was varied, the K_m for PRPP was found to increase as the QA concentration was decreased while V_{max} was unchanged (Figure 4B).

The substrate inhibition observed with PRPP was then investigated in more detail. The kinetic data show that V_{max} continues to increase with [PRPP] up to 5 mM (which is more than 200 times K_m). Normally one would expect the formation of a simple dead-end QPRTase:PRPP complex to cause V_{max} to plateau (as observed for the *Salmonella typhimurium* enzyme [29]). Above 0.3mM [PRPP] mixed inhibition was observed which suggests that PRPP not only binds to an active site (competitive) but to a second site which perturbs and inhibits the active site (non-competitive) (Figure 4C).

Site-directed mutagenesis

The mutants R138Q, K139A, K139S, R161Q and K171A, K171S completely abolished hQPRTase activity. Only three mutants retained any activity, R102Q, R102A and R161A with between 10 and 20% activity of wild type (Table 1). Further analysis of R161A confirmed that R161 is important for substrate binding.

Discussion

QPRTase catalyzes the transfer of the phosphoribosyl moiety from PRPP to QA yielding NAMN, pyrophosphate and CO_2. We have been unable to determine the hQPRTase structure with substrate or product bound; instead a tartrate molecule binds at the QA site mimicking in part QA. A structure alignment of hQPRTase with Mt-QPRTase revealed a very similar constellation of conserved residues at the active site. hQPRTase residues R102, R138, K139, R161, K171 and D222 are absolutely conserved. Mutagenesis analysis showed thatR138, K139, K171 are essential, whilst R161 and R102 are important for substrate recognition they are not absolutely required for activity. R138 is proposed[13] to stabilize the oxycarbonium ion which results from the ribosylphosphate S_N1 nucleophilic attack at the N atom of the pyridine ring (Figure 1)[7]. The formation of the anticipated intermediate is facilitated by the electron-withdrawing power of a metal ion and the *C3-exo* pucker of the ribosyl ring[13]. K139 and K171 are thought to be required for PRPP binding and interact with the phosphate groups during catalysis[13].

Steady-state kinetic studies on *E. coli* QPRTase had suggested an order in which PRPP binds first followed by QA to form the active ternary complex [28]. However, recent isotope partitioning studies on St-QPRTase and Mt-QPRTase suggested that the ordered sequence is binding of QA followed by PRPP [29]. Our analysis indicates that hQPRTase follows an ordered mechanism, QA binds first and PRPP second, in agreement with the bacterial enzymes. hQPRTase appears to be similar in efficiency to the bacterial enzymes. At higher PRPP concentrations substrate inhibition clearly occurs. The formation of a dead-end QPRTase:PRPP complex would result in simple competitive inhibition such as is seen in the bacterial (*S. typhimurium*) enzyme 29. However, in hQPRTase mixed inhibition is observed (Figure 4C). The occurrence of both non-competitive and competitive inhibition would suggest that PRPP in addition to binding the active site binds to another (second) site on the enzyme.

We speculate the hexameric structure seen for hQPRTase offers an explanation of the complex kinetics. The same hexameric arrangement has also been seen for Hp-QPRTase [16] and Tt-QPRTase (PDB code 1x1o) however neither enzyme has been kinetically characterized. The other bacterial structures form the canonical dimer. Although the crystal structure of Mt-QPRTase contains a hexamer in the asymmetric unit this is totally different from the human arrangement. Further PISA analysis of the Mt-QPRTase [34] structure agrees with the solution data that the enzyme is a dimer [15]. Within the canonical AB dimer the QA binding sites are separated by over 35 Å, however, the hexameric arrangement means the QA binding sites from different dimers (AB and CD dimer) are within 25 Å of each other. We note that the loop containing the catalytically important residue R161 is in contact with the loop from monomer A contact the same loop in monomer D (Figure 2C). It is possible that this contact would allow changes in the active site structure in response to PRPP binding in one subunit to be transmitted across this interface to the other subunit.

hQPRTase has a hexameric structure and exhibits complex kinetics. In humans QA is a powerful modulator of brain function and as hQPRTase is one of the key methods of controlling its concentration, some additional regulation of its activity may be desirable; we speculate that the hexameric arrangement may be important to this.

Materials and Methods

DNA and chemicals

Plasmid DNA containing hQPRTase (from human brain) was provided by Dr S.I. Fukuoka (Research Institute for Food Science, Kyoto University Uji, Japan). *E. coli* strain DH5α and BL21 (DE3) were purchased from Stratagene. All the restriction endonucleases, T4 DNA ligase and Vent DNA polymerase were purchased from either Promega or New England BioLabs. QA, NAMN and PRPP were purchased from Sigma. pEHISTEV plasmid (see On-line Supporting Materials 2)and plasmid expressing His-tagged TEV NIa protease were constructed in our laboratory for gene cloning, expression and purification. All other chemicals used in the crystallization were of the purest grade available from commercial sources.

Molecular biology

To construct the pEHIShqprt carrying the hQPRTase gene, the hQPRTase encoding sequence was generated using the 5′primer 5′CTAGTCATGAACGCTGAAGGCCTG3′ (*Bsp*HI site underlined) and the 3′ primer 5′ATGCGGATCCCTAGTGGATTTTGGGC 3′ (*Bam*HI site underlined) with a pBS plasmid containing full-length hQPRTase cDNA as the template [33]. The PCR-generated hQPRTase encoding sequences were digested with *Bsp*HI and *Bam*HI respectively. Vector pEHIShqprt was constructed by ligating *Bsp*HI/*Bam*HI-

digested the hQPRTase gene into a compatible *Nco*I/*Bam*HI-digested pEHISTEV vector. The DNA sequence of the hQPRTase gene in pEHIShqprt and the linkage regions were sequenced to confirm their integrity. The expressed hQPRTase in pEHIShqprt contains a six-histidine tag and a TEV protease cleavage site at its N-terminus. After the his-tag removal, the purified hQPRTase had extra two residues (glycine and alanine) attached to its N-terminus. Site directed mutagenesis was performed on a pEHIShqprt clone based on PCR-generated mutagenesis [35]. All the primers used were synthesized by Eurogentic. All the mutations and sequence integrity of the hQPRTase gene were confirmed by automated sequencing (Sequence Facility, University of Dundee).

Expression and purification of protein

To express hQPRTase, plasmid pEHIShqprt and the plasmids containing the hQPRTase gene with designed mutation were transformed into *E. coli* strain BL21(DE3). The transformed *E. coli* were grown in one liter of L-B medium containing 50μg/ml of kanamycin to an OD_{600}=0.6 and then induced with 0.4mM IPTG overnight at 20°C. The over-expressed 6xHis-tagged hQPRTases were purified by a nickel affinity column, a second step of nickel chromatography after TEV protease cleavage and then followed by gel filtration. The purified recombinant hQPRTase protein (containing extra glycine and alanine at its N-terminus) is concentrated into 10mg/ml and protein identity was confirmed by mass spectrometric analysis. The selenomethionine variant was expressed using methionine biosynthesis inhibition [36]. The purification of selenomethionine variant was carried out essentially as that of the native except the purification buffer containing 5mM 2-mercaptomethanol. The selenomethionine variant protein behaved exactly as the native in purification and crystallization experiments.

Activity assays

The initial activity of human QPRTase was determined using an HPLC assay that measured the formation of nicotinic acid mononucleotide essentially as described, [27], while a continuous UV spectrophotometric assay as reported by Cao *et al* [29] using a Uvikon spectrophotometer (Model 930) was employed for kinetic studies. The HPLC system consisted of a Cecil 1200 variable wavelength detector and a Phenosphere 5 μ C18 column (150 × 4.6 mm) with an integral guard column. The mobile phase contained *t*-butyl ammonium hydrogen sulfate (0.02 M) in ammonium dihydrogen phosphate (0.2 M), pH 5.3. The flow rate was set to 0.6 mL/min^{-1} with a detection wavelength of 254 nm. Under these conditions NAMN and QA were eluted at 11:3 and 4:0 minutes respectively. Thymidine monophosphate was used as an internal standard with a retention time of 17.20 minutes. A typical assay mixture contained 50 mM K_2HPO_4/KH_2PO_4, 6 mM $MgCl_2$, 0.3 mM quinolinic acid and 1 mM PRPP in a total volume of 550 μl (pH 7.2). Each assay was initiated by adding 7 μg of purified hQPRTase and the mixture was incubated at 37 °C for 20 min and then applied to the HPLC. In the UV based-assay the formation of the product was measured at 266 nm (based on the difference in extinction coefficients between QA and NAMN (ΔA_{266} = 920 M cm^{-1}). Typical assay mixtures contained 50 mM K_2HPO_4/ KH_2PO_4, 6 mM $MgCl_2$, 0.3 mM quinolinic acid and 0.1 mM PRPP in a total volume of 1 ml (pH 7.2). After adding 14 μg of QPRTase, the mixtures were incubated at 37 °C for 30 min. To determine Km values for each substrate the concentrations were varied. The absorbance was then measured over 30 minutes at 266 nm at 37 °C. Each data point was measured in triplicate. Kinetic parameters were calculated using GraphPad Prism 3 program using non-linear regression analysis of the triplicate experimental data. Lineweaver-Burke plots are shown for illustrative purposes only

Structural Biology

Initial crystallization conditions were obtained with sitting-drop vapor diffusion using Crystal Screen kits (Hampton Research) at 20 °C with a protein concentration of 10 mg ml^{-1}. Crystals appeared within 5 days in condition 29 of Hampton Screen 1. Refinement of these conditions yielded single crystals from a mixture of 2 μl of the protein (10mg ml^{-1} pH 7.5 50 mM Tris) and 2 μl of precipitant 0.6 M K. Na tartrate, 0.1 M Na. Hepes, pH 7.6. The crystal was soaked with 20 % (v/v) glycerol and mounted in a loop then immediately cooled to 100 K by a stream of nitrogen. Diffraction data were collected at ESRF beamline ID14-1 as a total of 360 10 s 0.5 ° oscillations. The data were indexed and integrated using *MOSFLM* and scaled together using *SCALA* [37] A data set to 2.0 Å was recorded and the space group determined as $P2_12_12_1$. Attempts to solve the structure with the bacterial enzymes as search models failed. To determine the phase, Se-Met crystals were obtained as described for the native protein. A three wavelength MAD data set was collected at ESRF beamline BM14 with a resolution of 2.4 Å. 34 Se atom sites were located by SHELXD [38] but initial phases (figure of merit 0.5 to 3.0 Å) were too poor to trace the structure. Manual inspection was used to determine the non-crystallographic symmetry operators from the Se positions. Twelve fold non-crystallographic averaging (the initial correlation between subunits ranged from 0.15 to 0.25, although this rapidly improved with refinement of operators) coupled to solvent flattening and extension to 2.0 Å with DM [39] produced a map which was easily traced. The structure was refined using REFMAC5 [40] and manually rebuilt with COOT [41]. The full details of the X-ray data are listed in Table 2.

Supplementary Material

Refer to Web version on PubMed Central for supplementary material.

Acknowledgments

We thank Dr S.I. Fukuoka, for providing the cloned hQPRTase gene and specific anti-hQPRTase serum, and Dr Catherine Botting, for mass spectrometric analysis. Structural biology was carried out the Scottish Structural Proteomics Facility which is funded by the Biotechnology and Biological Science Research Council and the Scottish Funding Council.

References

1. Iwai K, Taguchi H. Distribution of quinolinate phosphoribosyl-transferase in animals, plants and microorganisms. J Nutr Sci Vitaminol (Tokyo). 1973; 19:491–9. [PubMed: 4799479]
2. Foster AC, Whetsell WO Jr. Bird ED, Schwarcz R. Quinolinic acid phosphoribosyltransferase in human and rat brain: activity in Huntington's disease and in quinolinate-lesioned rat striatum. Brain Res. 1985; 336:207–14. [PubMed: 3159462]
3. Feldblum S, Rougier A, Loiseau H, Loiseau P, Cohadon F, Morselli PL, Lloyd KG. Quinolinic-phosphoribosyl transferase activity is decreased in epileptic human brain tissue. Epilepsia. 1988; 29:523–9. [PubMed: 3409840]
4. Foster AC, Schwarcz R. Characterization of quinolinic acid phosphoribosyltransferase in human blood and observations in Huntington's disease. J Neurochem. 1985; 45:199–205. [PubMed: 2582090]
5. Speciale C, Okuno E, Schwarcz R. Increased quinolinic acid metabolism following neuronal degeneration in the rat hippocampus. Brain Res. 1987; 436:18–24. [PubMed: 2961415]
6. Nakagawa Y, Asai H, Kitoh J, Mori H, Nakano K. Increase in the level of mRNA for 3-hydroxyanthranilate 3,4-dioxygenase in brain of epilepsy-prone El mice. Biosci Biotechnol Biochem. 1995; 59:2191–2. [PubMed: 8541664]
7. Tao W, Grubmeyer C, Blanchard JS. Transition state structure of Salmonella typhimurium orotate phosphoribosyltransferase. Biochemistry. 1996; 35:14–21. [PubMed: 8555167]

8. Scapin G, Grubmeyer C, Sacchettini JC. Crystal structure of orotate phosphoribosyltransferase. Biochemistry. 1994; 33:1287–94. [PubMed: 8312245]

9. Eads JC, Scapin G, Xu Y, Grubmeyer C, Sacchettini JC. The crystal structure of human hypoxanthine-guanine phosphoribosyltransferase with bound GMP. Cell. 1994; 78:325–34. [PubMed: 8044844]

10. Smith JL. Glutamine PRPP amidotransferase: snapshots of an enzyme in action. Curr Opin Struct Biol. 1998; 8:686–94. [PubMed: 9914248]

11. Schumacher MA, Carter D, Scott DM, Roos DS, Ullman B, Brennan RG. Crystal structures of Toxoplasma gondii uracil phosphoribosyltransferase reveal the atomic basis of pyrimidine discrimination and prodrug binding. Embo J. 1998; 17:3219–32. [PubMed: 9628859]

12. Eriksen TA, Kadziola A, Bentsen AK, Harlow KW, Larsen S. Structural basis for the function of Bacillus subtilis phosphoribosyl-pyrophosphate synthetase. Nat Struct Biol. 2000; 7:303–8. [PubMed: 10742175]

13. Eads JC, Ozturk D, Wexler TB, Grubmeyer C, Sacchettini JC. A new function for a common fold: the crystal structure of quinolinic acid phosphoribosyltransferase. Structure. 1997; 5:47–58. [PubMed: 9016724]

14. Smith JL. Forming and inhibiting PRT active sites. Nat Struct Biol. 1999; 6:502–4. [PubMed: 10360346]

15. Sharma V, Grubmeyer C, Sacchettini JC. Crystal structure of quinolinic acid phosphoribosyltransferase from Mmycobacterium tuberculosis: a potential TB drug target. Structure. 1998; 6:1587–99. [PubMed: 9862811]

16. Kim MK, Im YJ, Lee JH, Eom SH. Crystal structure of quinolinic acid phosphoribosyltransferase from Helicobacter pylori. Proteins. 2006; 63:252–5. [PubMed: 16419067]

17. Schwarzenbacher R, Jaroszewski L, von Delft F, Abdubek P, Ambing E, Biorac T, Brinen LS, Canaves JM, Cambell J, Chiu HJ, Dai X, Deacon AM, DiDonato M, Elsliger MA, Eshagi S, Floyd R, Godzik A, Grittini C, Grzechnik SK, Hampton E, Karlak C, Klock HE, Koesema E, Kovarik JS, Kreusch A, Kuhn P, Lesley SA, Levin I, McMullan D, McPhillips TM, Miller MD, Morse A, Moy K, Ouyang J, Page R, Quijano K, Robb A, Spraggon G, Stevens RC, van den Bedem H, Velasquez J, Vincent J, Wang X, West B, Wolf G, Xu Q, Hodgson KO, Wooley J, Wilson IA. Crystal structure of a type II quinolic acid phosphoribosyltransferase (TM1645) from Thermotoga maritima at 2. A resolution. Proteins. 2004; 55:768–71.

18. Packman PM, Jakoby WB. Crystalline quinolinate phosphoribosyltransferase. J Biol Chem. 1965; 240:4107–8. [PubMed: 5320648]

19. Hughes KT, Dessen A, Gray JP, Grubmeyer C. The Salmonella typhimurium nadC gene: sequence determination by use of Mud-P22 and purification of quinolinate phosphoribosyltransferase. J Bacteriol. 1993; 175:479–86. [PubMed: 8419294]

20. Taguchi H, Iwai K. Characteristics of quinolinate phosphoribosyltransferase from the “Shiitake” mushroom (Lentinus edodes). J Nutr Sci Vitaminol. 1974; 20:283–91. [PubMed: 4373552]

21. Taguchi H, Iwai K. Purification and properties of quinolinate phosphoribosyltransferase from the “Shiitake” mushroom (Lentinus edodes). J Nutr Sci Vitaminol. 1974; 20:269–81. [PubMed: 4373551]

22. Sinclair SJ, Murphy KJ, Birch CD, Hamill JD. Molecular characterization of quinolinate phosphoribosyltransferase (QPRtase) in Nicotiana. Plant Mol Biol. 2000; 44:603–17. [PubMed: 11198422]

23. Iwai K, Taguchi H. Purification and crystallization of quinolinate phosphoribosyltransferase from hog liver. Biochem Biophys Res Commun. 1974; 56:884–91. [PubMed: 4826469]

24. Foster AC, Zinkand WC, Schwarcz R. Quinolinic acid phosphoribosyltransferase in rat brain. J Neurochem. 1985; 44:446–54. [PubMed: 2578178]

25. Okuno E, White RJ, Schwarcz R. Quinolinic acid phosphoribosyltransferase: purification and partial characterization from human liver and brain. J Biochem (Tokyo). 1988; 103:1054–9. [PubMed: 3139649]

26. Kohler C, Eriksson LG, Flood PR, Hardie JA, Okuno E, Schwarcz R. Quinolinic Acid Metabolism in the Rat-Brain - Immunohistochemical Identification of 3-Hydroxyanthranilic Acid Oxygenase

and Quinolinic Acid Phosphoribosyltransferase in the Hippocampal Region. Journal of Neuroscience. 1988; 8:975–987. [PubMed: 3346732]

27. Kalikin L, Calvo KC. Inhibition of quinolinate phosphoribosyl transferase by pyridine analogs of quinolinic acid. Biochem Biophys Res Commun. 1988; 152:559–64. [PubMed: 2452632]
28. Bhatia R, Calvo KC. The sequencing expression, purification, and steady-state kinetic analysis of quinolinate phosphoribosyl transferase from Escherichia coli. Arch Biochem Biophys. 1996; 325:270–8. [PubMed: 8561507]
29. Cao H, Pietrak BL, Grubmeyer C. Quinolinate phosphoribosyltransferase: kinetic mechanism for a type II PRTase. Biochemistry. 2002; 41:3520–8. [PubMed: 11876660]
30. Okuno E, Schwarcz R. Purification of quinolinic acid phosphoribosyltransferase from rat liver and brain. Biochim Biophys Acta. 1985; 841:112–9. [PubMed: 3926003]
31. Iwai K, Taguchi H. Crystallization and properties of quinolinate phosphoribosyltransferase from hog liver. Methods Enzymol. 1980; 66:96–101. [PubMed: 7374514]
32. Moore D, Bice T, Jin L, Grandhi A, DeLucas LJ, Narayana SV. Crystallization and preliminary crystallographic investigation of porcine quinolinate phosphoribosyltransferase. Acta Crystallogr D Biol Crystallogr. 1998; 54(Pt 1):119–20. [PubMed: 9761830]
33. Fukuoka SI, Nyaruhucha CM, Shibata K. Characterization and functional expression of the cDNA encoding human brain quinolinate phosphoribosyltransferase. Biochim Biophys Acta. 1998; 1395:192–201. [PubMed: 9473669]
34. Krissinel, E.; Henrick, K. Detection of Protein Assemblies in Crystals. In: Berthold, MR., editor. CompLife 2005, LNBI 3695, pp. 163--174. Springer-Verlag Berlin Heidelberg. Springer-Verlag; Berlin Heidelberg: 2005. p. 163-174.
35. Brons-Poulsen J, Petersen NE, Horder M, Kristiansen K. An improved PCR-based method for site directed mutagenesis using megaprimers. Mol Cell Probes. 1998; 12:345–8. [PubMed: 9843651]
36. Doublie S. Preparation of selenomethionyl proteins for phase determination. Macromolecular Crystallography. 1997; Pt A 276:523–530.
37. Picot D, Loll PJ, Garavito RM. The X-Ray Crystal-Structure of the Membrane-Protein Prostaglandin-H(2) Synthase-1. Nature. 1994; 367:243–249. [PubMed: 8121489]
38. Schneider TR, Sheldrick GM. Substructure solution with SHELXD. Acta Cryst. D. 2002; 58:1772–1779. [PubMed: 12351820]
39. Cowtan K. ‘dm’: An automated procedure for phase improvement by density modification. Joint CCP4 and ESF-EACBM Newsletter on Protein Crystallography. 1994; 31:34–38.
40. Murshudov GN, Vagin AA, Dodson EJ. Refinement of macromolecular structures by the maximum-likelihood method. Acta Cryst. D. 1997; 53:240–255. [PubMed: 15299926]
41. Emsley P, Cowtan K. Coot: model-building tools for molecular graphics. Acta Cryst. D. 2004; 60:2126–2132. [PubMed: 15572765]
42. Davis IW, Murray LW, Richardson JS, Richardson DC. MolProbity: structure validation and all-atom contact analysis for nucleic acids and their complexes. Nucleic Acids Res. 2004; 32:W615–W619. [PubMed: 15215462]

Europe PMC Funders Author Manuscripts

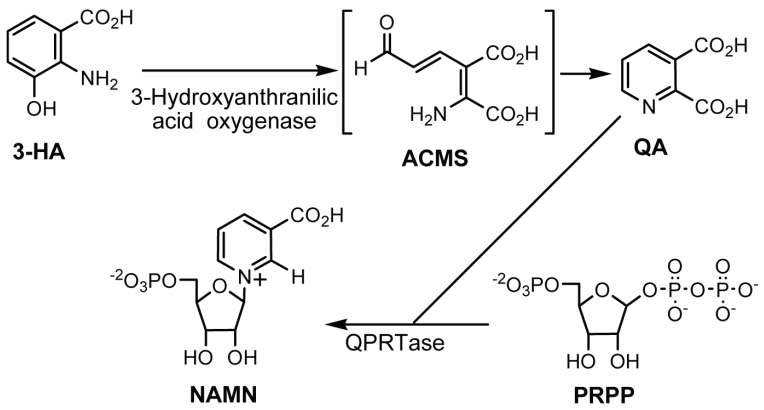

Figure 1.
Schematic representation of the quinolinic acid biosynthetic pathway.

Europe PMC Funders Author Manuscripts

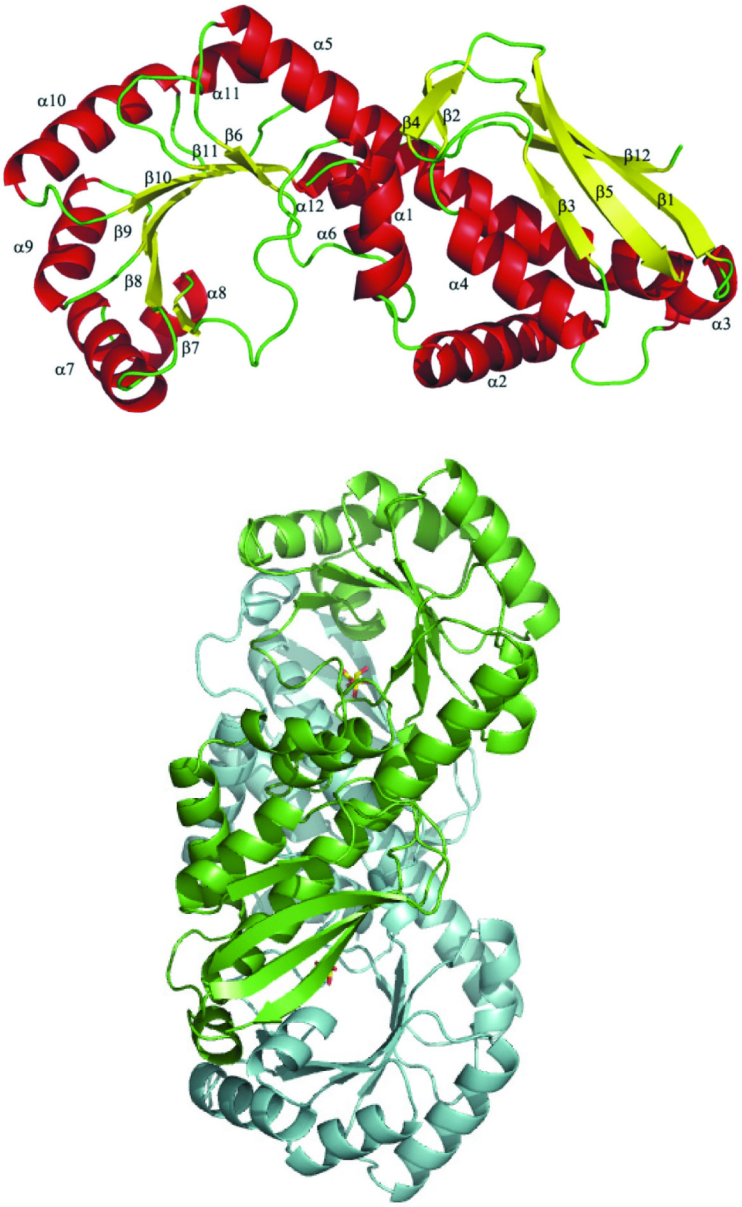

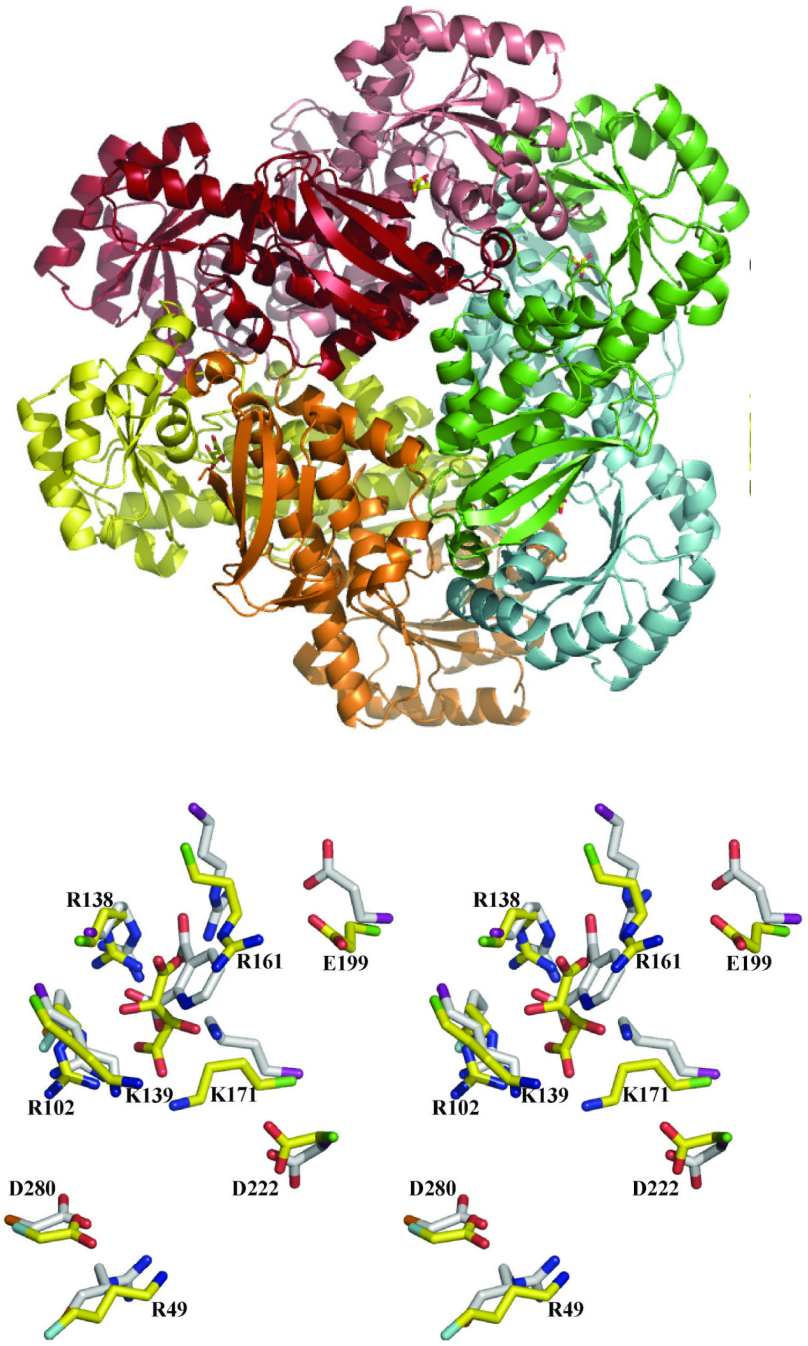

Figure 2.

The structure of hQPRTase. A) The hQPRTase monomer. The helices are shown in red, beta sheets are in yellow and loops are in blue. B) The hQPRTase dimer which is also found in bacterial enzymes. Monomer A is shown in green while monomer B is colored cyan. Tartaric acid is shown as sticks (oxygen colored red and carbon colored yellow) and locates the active site. C) Ribbon diagram of the hQPRTase hexamer in the asymmetric unit, monomers A and B are colored as (b), monomers C, D, E and F are colored deep red, salmon, yellow and orange respectively. The three fold axis is perpendicular to the plane of the paper, the three two folds lie in the plane giving the hexamer D3 symmetry. D)

Superposition of hQPRTase and the Mt-QPRTase QA complex (PDB 1QPQ) active sites. Atoms are colored as 2b, except Mt-QPRTase carbons are shown in light grey. The key conserved residues are shown, as are QA and tartaric acid. The residues that form the active site come from both monomers in the dimer, to show this in hQPRTase the Cα atoms are colored green (monomer A) and cyan (monomer B). In Mt-QPRTase, Cα is colored purple in monomer A and orange in monomer B.

Europe PMC Funders Author Manuscripts

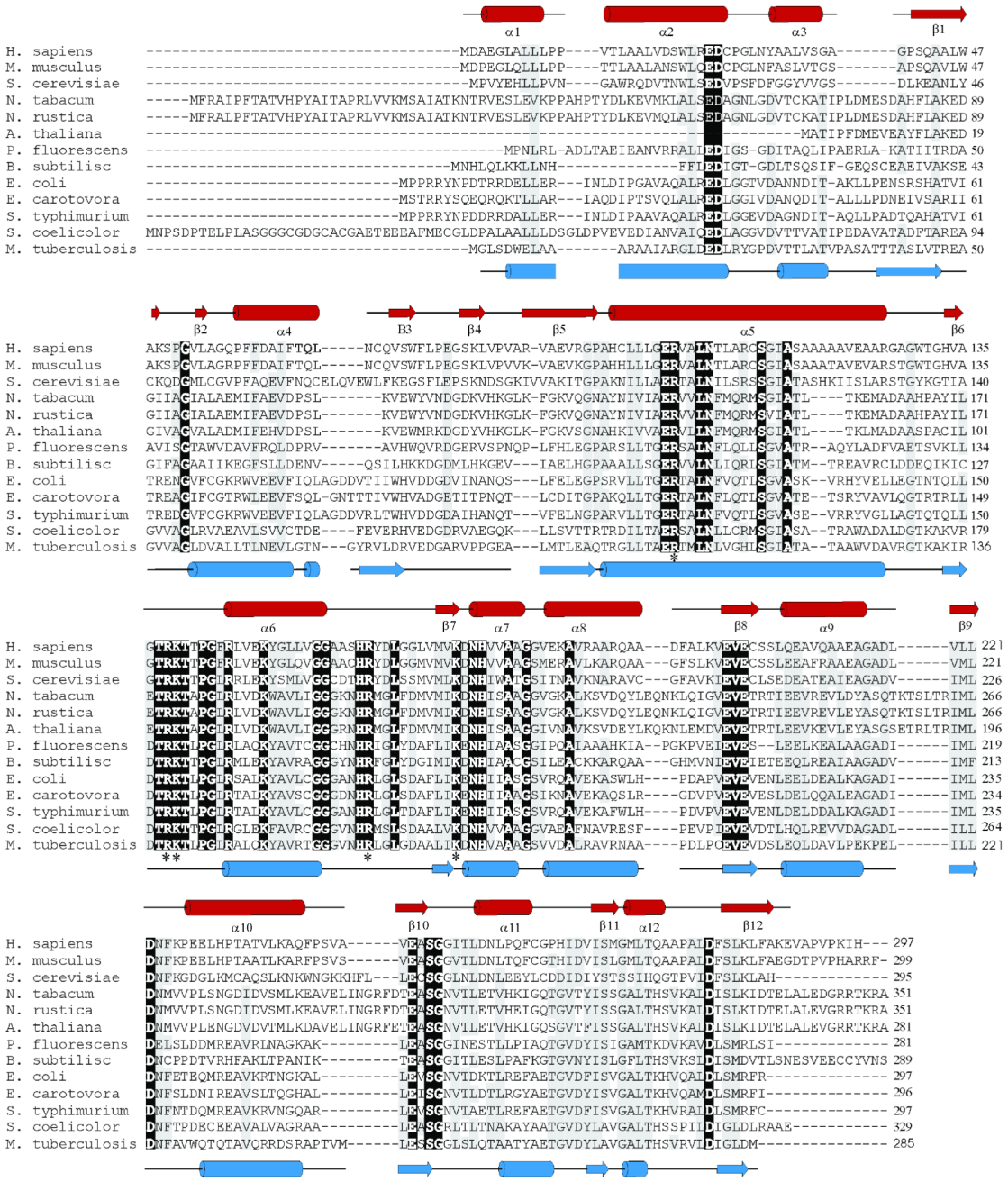

Figure 3.

Sequence alignment of the hQPRTase homologs. Conserved residues are highlighted in black and mutagenesis analyzed residues are marked with asterisks. The secondary structure elements of hQPRTase are shown above the alignment while those of Mt-QPRTase are shown below; Helices are represented as rectangles and strands as arrows. The aligned sequences and their access numbers are, *Homo sapiens* (Q15274), *Mus musculus* (Q91X91), *Saccharomyces cerevisiae* (NP 602317), *Nicotiana tabacum* (BAA92153), *Nicotiana rustica* (CAB59429), *Thermotoga maritime* (1O4U). *Helicobacter pylori* (2B7Q), *Thermus thermophilus* (1X1O), *Escherichia coli* (AAB00467), *Erwinia carotovora* (CAG76696), *Salmonella typhimurium* (1QAP), *Streptomyces coelicolor* (NP 627589) *and*

Mycobacterium tuberculosis (1QPQ). Sequences were aligned using the program BioEdit version 4.8.10.

Europe PMC Funders Author Manuscripts

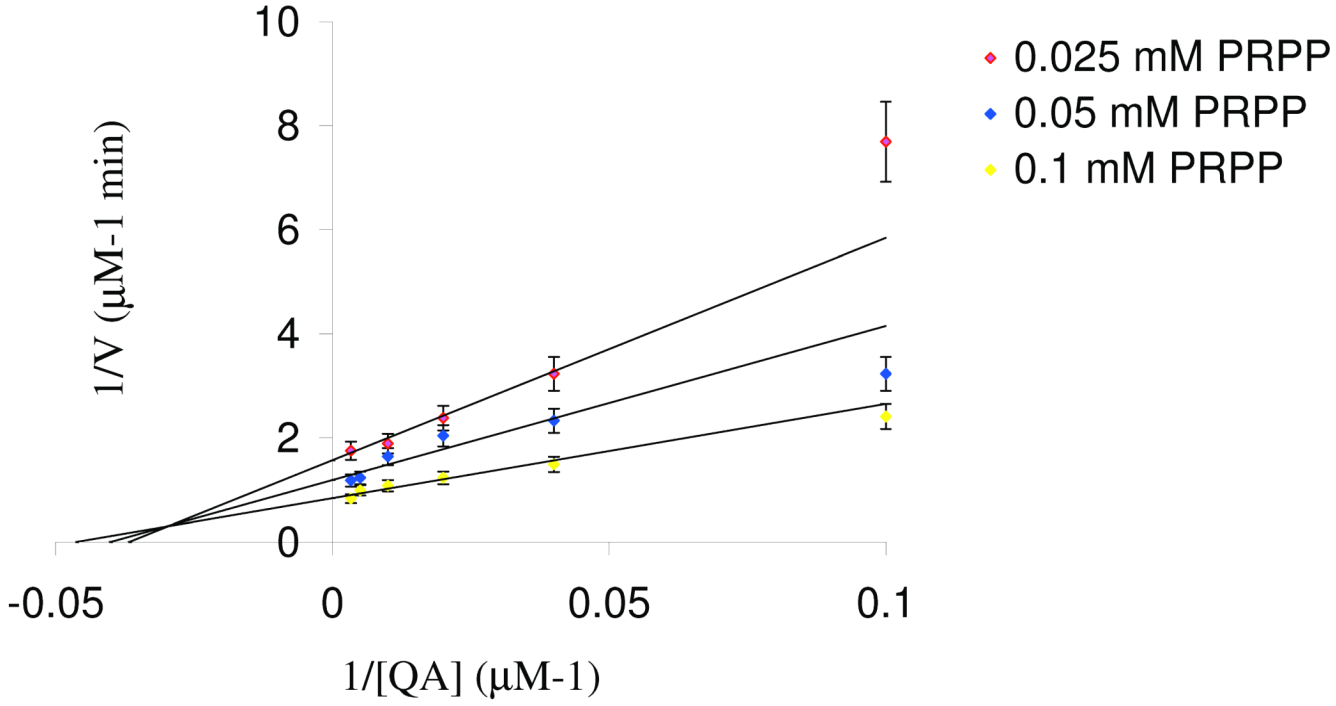

Europe PMC Funders Author Manuscripts

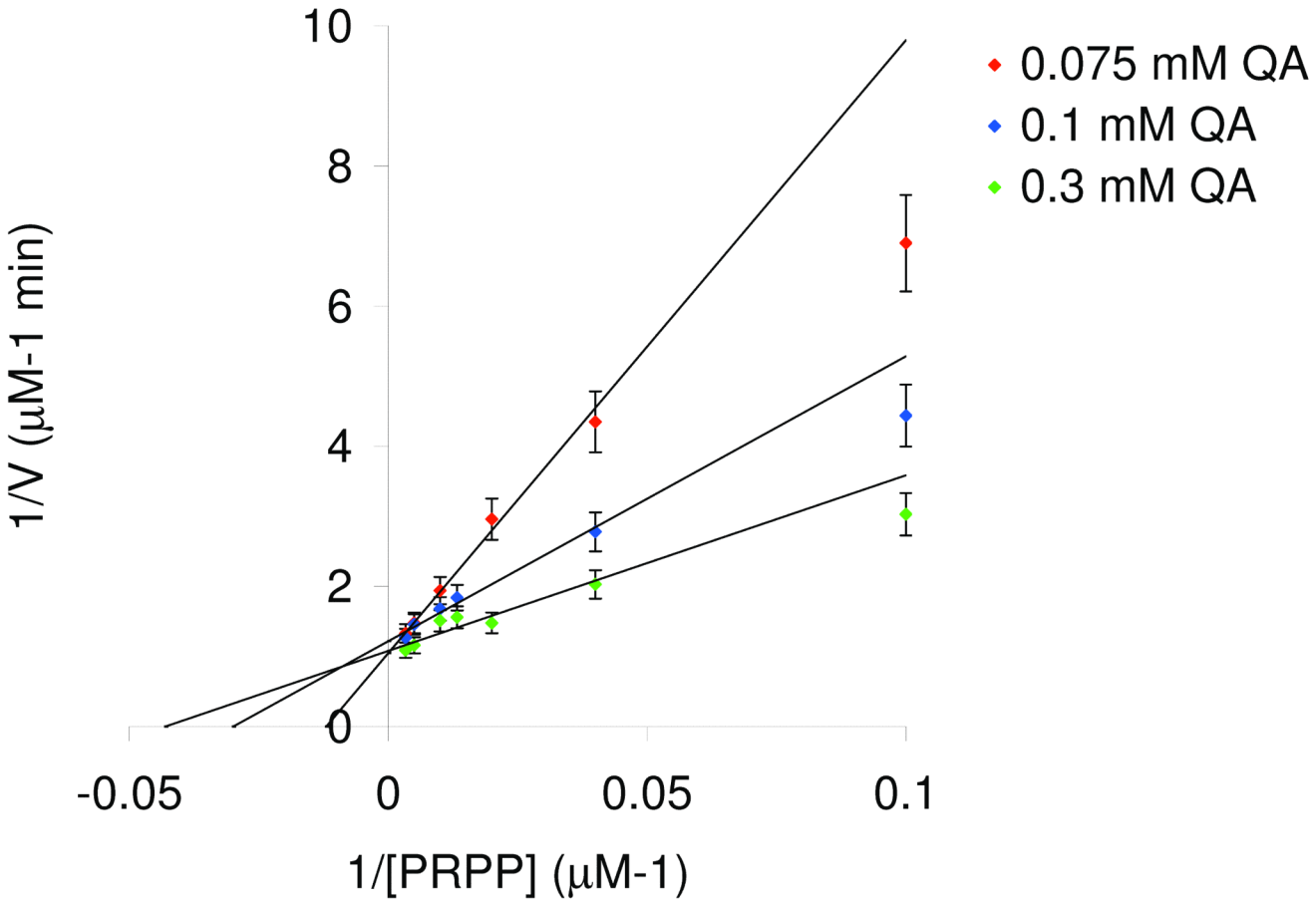

Europe PMC Funders Author Manuscripts

Europe PMC Funders Author Manuscripts

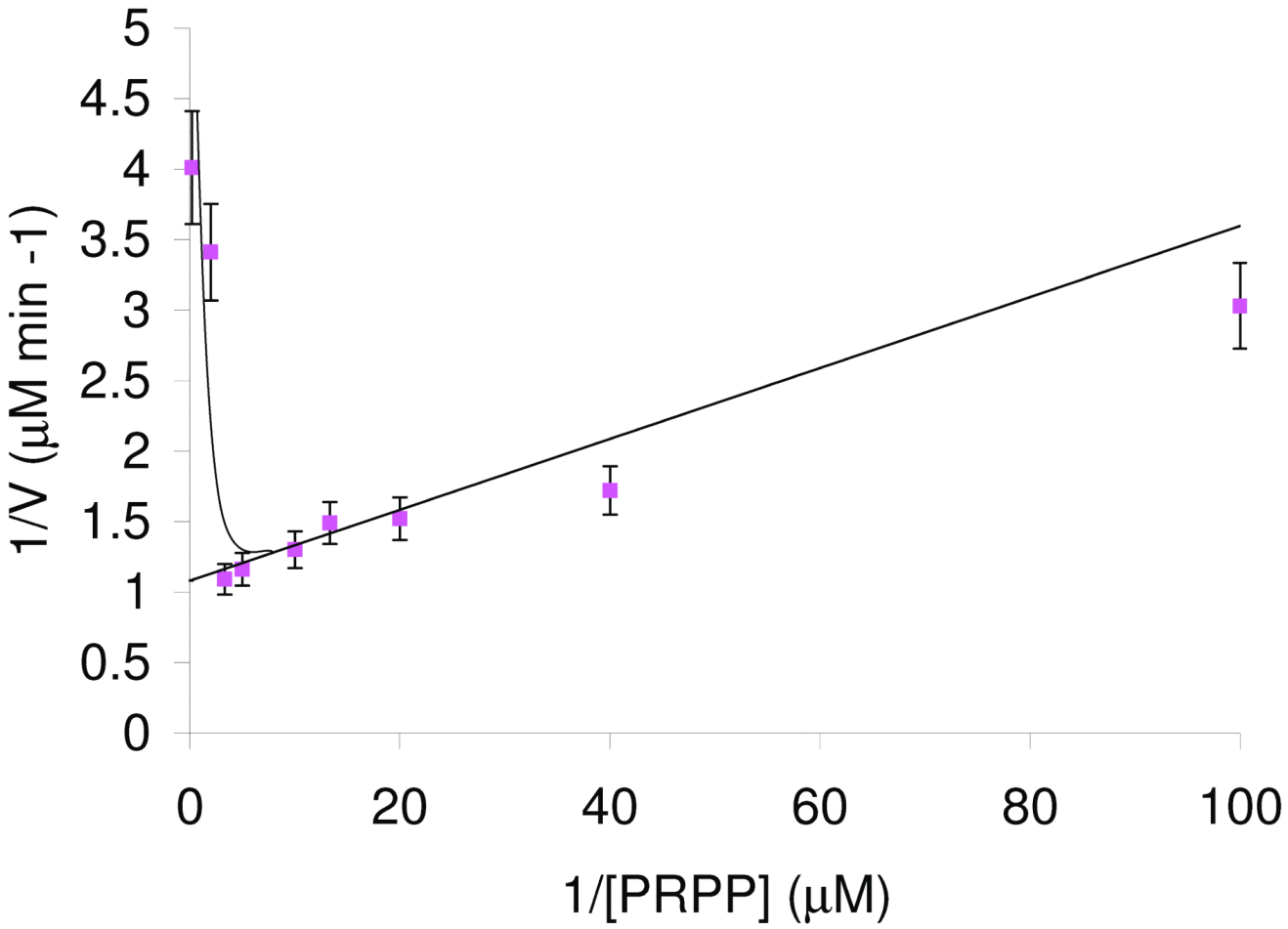

Figure 4.

Effect of PRPP and QA concentration on the rate of formation of NAMN catalyzed by purified hQPRTase. A) Lineweaver-burk plots for QA as the variable substrate at a range of fixed PRPP concentrations. Reaction mixtures with a total volume of 1 ml contained 50 mM K_2HPO_4/KH_2PO_4, pH 7.2, 6 mM $MgCl_2$, QA and PRPP concentrations as described. B) Lineweaver-burk plots for PRPP as the variable substrate at a range of fixed QA concentrations. Reaction mixtures with a total volume of 1ml contained 50 mM K_2HPO_4/KH_2PO_4, pH 7.2, 6 mM $MgCl_2$, 0.1 mM PRPP and the concentration of QA as described. C) Lineweaver-burk plot for PRPP as the variable substrate over an extended concentration range (0.01 to 5.0 mM). Inhibition is mixed. Reaction mixtures with a total volume of 1ml contained 50 mM K_2HPO_4/KH_2PO_4, pH 7.2, 6 mM $MgCl_2$, 0.3 mM QA and the concentration of PRPP as described in the text.

Europe PMC Funders Author Manuscripts

Table 1

Kinetic data for native QPRTase and mutant enzymes

Enzyme	Relative activity[a] (%)	Km for QA (μM)	Vmax for QA (μM min^{-1})
Native	100	21.6 ± 3.0	1.19 ± 0.05
R161A	20	319 ± 60	0.71 ± 0.
R161Q	Not detected	-	-
R102A	10	not measured	not measured
R102Q	10	not measured	not measured
R138Q	Not detected	-	-
K171A	Not detected	-	-
K171S	Not detected	-	-
K139A	Not detected	-	-
K139S	Not detected	-	-

[a]Assays were carried out in a 1ml solution containing 50 mM K_2HPO_4/KH_2PO_4 buffer pH 7.2, 0.3 mM quinolinic acid, 0.1 mM PRPP and 6mM MgCl2. Reaction was initiated by the addition of 14 μg of the mutant QPRTase enzyme.

Table 2

Summary of crystallographic statistics.

	Native	MAD		
		Peak	Remote	Inflection
Wavelength (Å)	0.932	0.9792	0.8983	0.9793
Resolution(Å)	61-2.0 (2.1-2.0)	53.4-2.5	48.8-2.4	53.4-2.5
Space group		$P2_12_12_1$		
Unit-cell (Å)	a=111.5 b=179.5 c =194.7	a=111.2, b=180.8, c=196.1		
Unique reflections	261406	88253	87096	87782
multiplicity	3.6 (3.0)	6.9	3.7	3.8
Completeness (%)	89.4 (72)	99.9	98.7	99.4
R_{merge} (%)	6.9 (32)	8.3	6.9	7.0
I/σI	11.6 (2.8)	6.8	7.1	7.3
Wilson B-factor	19			
Refinement				
R/ R-free	17.7 / 20.8 (22.7 / 26.9)			
R_{msd}				
Bonds (Å)/ angles (°)	0.01 / 1.2			
NCS main chain	0.06 / 0.4			
Core (Å)/ loop (Å)[a]				
Average B-factors				
25308 protein atoms	9			
3000 water atoms	22			
120 tartrate atoms	19			
Ramachandran				
Favored (%)/ outlier (%)[b]	98.6 / 0			
PDB code	2jbm			

[a]Main chain atoms, N, Cα, C and O. 236 residues were judged core and tightly restrained to obey non –crystallographic symmetry, 47 residues were judged flexible loops and less tightly restrained, 12 residues were not restrained to non-crystallographic symmetry.

[b]MOLPROBITY [42] definition of favored and outlier